Journal of Hazardous Materials 443 (2023) 130363

Contents lists available at ScienceDirect

Journal of Hazardous Materials

journal homepage: www.elsevier.com/locate/jhazmat

# Activation of chloride by oxygen vacancies-enriched $TiO_2$ photoanode for efficient photoelectrochemical treatment of persistent organic pollutants and simultaneous $H_2$ generation

Jiabao Wu [b,1], Ying Tao [b,1], Chi Zhang [b], Qiong Zhu [b], Dieqing Zhang [a,*], Guisheng Li [a,b,c,**]

[a] The Education Ministry Key Lab of Resource Chemistry, Shanghai Key Laboratory of Rare Earth Functional Materials, Shanghai Normal University, Shanghai 200234, PR China
[b] School of Environmental and Geographical Sciences, Shanghai Normal University, Shanghai 200234, PR China
[c] School of Materials and Chemistry, University of Shanghai for Science and Technology, Shanghai 200093, PR China

## HIGHLIGHTS

- A PEC-Cl system was proposed for efficient degradation POPs and generation of $H_2$.
- Mechanism of $Cl^-$ activation in $O_v$-$TiO_2$/PEC-Cl system was revealed.
- The oxygen vacancies in $O_v$-$TiO_2$ reduced the activation energy of $Cl^-$ and $H_2O$.
- ClO• radical was the main RCS responsible for the degradation of POPs.
- Nearly no toxic by-product of chlorates was produced in the PEC-Cl system.

## GRAPHICAL ABSTRACT

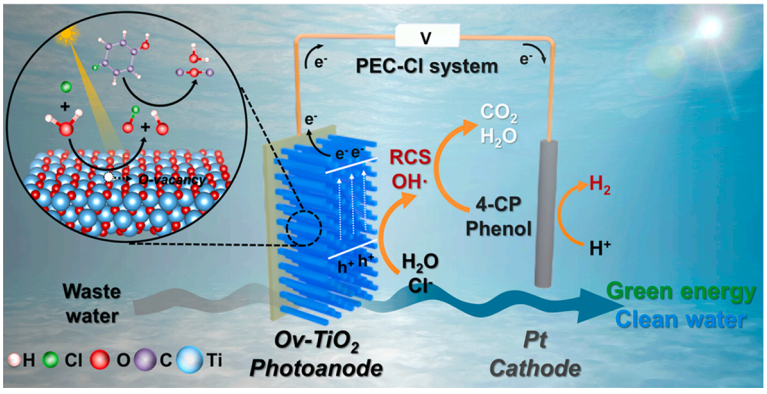


## ARTICLE INFO

Editor: Sungjun Bae

*Keywords:*
Industrial saline organic wastewater
Reactive chlorine specie
Photoelectrochemical chlorine system
Oxygen vacancies
Toxic by-product

## ABSTRACT

Photoelectrochemical (PEC) activation of chloride ions ($Cl^-$) to degrade persistent organic pollutants (POPs) is a promising strategy for the treatment of industrial saline organic wastewater. However, the wide application of this technology is greatly restricted due to the general photoanode activation of $Cl^-$ with poor capability, the propensity to produce toxic by-products chlorates, and the narrow pH range. Herein, oxygen vacancies-enriched titanium dioxide ($O_v$-$TiO_2$) photoanode is explored to strongly activate $Cl^-$ to drive the deep mineralization of POPs wastewater in a wide pH range (2−12) with simultaneous production of $H_2$. More importantly, nearly no toxic by-product of chlorates was produced during such PEC-Cl system. The degradation efficiency of 4-CP and $H_2$ generation rate by $O_v$-$TiO_2$ were 99.9% within 60 min and 198.2 μmol $h^{-1}$ $cm^{-2}$, respectively, which are far superior to that on the $TiO_2$ (33.1% within 60 min, 27.5 μmol $h^{-1}$ $cm^{-2}$) working electrode. DFT calculation and

* Corresponding author.
** Corresponding author at: The Education Ministry Key Lab of Resource Chemistry, Shanghai Key Laboratory of Rare Earth Functional Materials, Shanghai Normal University, Shanghai 200234, PR China.
*E-mail addresses:* dqzhang@shnu.edu.cn (D. Zhang), liguisheng@shnu.edu.cn (G. Li).
[1] Equal contribution

https://doi.org/10.1016/j.jhazmat.2022.130363
Received 5 September 2022; Received in revised form 6 November 2022; Accepted 7 November 2022
Available online 9 November 2022

capture experiments revealed that $O_v$-$TiO_2$ with abundant oxygen vacancies is conducive to the activation of $Cl^-$ to produce more reactive chlorine species, evidenced by its high production of free chlorine (48.7 mg $L^{-1}$ vs 7.5 mg $L^{-1}$ of $TiO_2$). The as-designed PEC-Cl system in this work is expected to realize the purification of industrial saline organic wastewater coupling with green energy $H_2$ evolution.

## 1. Introduction

The high-speed development of industrialization has produced a large amount of saline organic wastewater, leading to severe water contamination and threatening human health (Jassby et al., 2018; Song et al., 2021; Lin et al., 2020). Recently, several sewage treatment technologies have emerged, including physical adsorption method (Sun et al., 2020; Pu et al., 2018), membrane treatment technology (Pan et al., 2020; Chen et al., 2021a), chemical oxidation method (Li et al., 2021a; Sözen et al., 2019; Ke et al., 2021), biodegradation method (Jayakumar et al., 2021; Bilal et al., 2022; Frank et al., 2021; Liu et al., 2022). Unfortunately, all of these methods have limitations due to the high salt content of wastewater and the wide variation in pH, which is the handicap of industrial saline organic wastewater treatment.

Photoelectrochemical (PEC) technology (Pan et al., 2019; Kim et al., 2018; Luo et al., 2017; Dai et al., 2020; Wang et al., 2020) has aroused extensive attention as one of the most promising approaches for wastewater treatment and synergistic generation of $H_2$ by using solar energy and external bias due to its merits of high-stability electrodes that can be used in wide pH environment (Zheng et al., 2021; Zheng and Lo, 2021). As for saline organic wastewater, in addition to the reactive oxygen species (ROS) produced by photogenerated holes oxidation (Lian et al., 2020; Nosaka and Nosaka, 2017; Liu et al., 2020; Chen et al., 2021b; Zhao et al., 2019; Mei et al., 2021), the enriched $Cl^-$ can also be oxidized to reactive chlorine species (RCS) (Li et al., 2020; Ji et al., 2017; Menzel et al., 2013; Koo et al., 2019; Cheng et al., 2020; Zhang et al., 2019), such as chlorine radical (Cl•, $Cl_2^{\bullet-}$), chlorine oxygen free (ClO•) and free chlorine ($Cl_2$, HClO/$ClO^-$) (FCS). Both ROS and RCS are strong oxidants that can efficiently break down various organic pollutants, enabling a collaborative wastewater treatment strategy. However, the traditional PEC-Cl systems (usually based on photoanodes such as $TiO_2$, $WO_3$ and $BiVO_4$) (Kim et al., 2018; Koo et al., 2019; Li et al., 2021b) are faced to many challenges including easy recombination of photocarriers, narrow range of pH, poor activation ability of $Cl^-$ and excessive oxidation of $Cl^-$ by HO• to produce toxic by-products chlorate ($ClO_3^-$, $ClO_4^-$) (Chen et al., 2017; Hou et al., 2018; Coates and Achenbach, 2004), which limit their practical application in wastewater treatment.

Defect engineering, especially oxygen vacancies, is ubiquitous in metal oxides and has profound effects on optical, physical and catalytic properties of materials (Kim et al., 2022; Ma et al., 2022). The oxygen vacancy can improve the molecular adsorption characteristics and the reaction activity on the surface of the photoelectrode, narrow the band gap to expand the absorption of light, increase the carrier concentration, improve the conductivity and charge separation efficiency (Wang et al., 2012; Wang et al., 2018a; Wang et al., 2019). Meanwhile, oxygen vacancies also have certain advantages in the activation of free radicals. Li et al. reported that in the activation process of hydrogen peroxide ($H_2O_2$), the oxygen vacancy accelerated the electron transfer between the catalyst and $H_2O_2$, lowered the reaction energy barrier, and activated $H_2O_2$ very effectively, and thus improved the reaction kinetics (Li et al., 2017). Lim et al. showed that oxygen vacancies provide catalytic sites for $HSO_5^-$ transformation and promote the production of $SO_4^{\bullet-}$ radicals during PMS activation (Lim et al., 2019). Oxygen vacancies not only improve the photoelectrochemical properties of the photoelectrode itself, but also increase the adsorption and activation sites of molecules, which are conducive to the production of highly active free radicals on the surface of the photoanode.

Herein, we used $TiO_2$ as a model catalyst to introduce appropriate oxygen vacancies in $TiO_2$ nanorods with high specific surface area, sufficient reaction sites and favorable free radical transfer to verify the PEC active chlorine system (PEC-Cl). The experimental results showed that the introduction of oxygen vacancy can produce a large amount of RCS, which can effectively degrade POPs and generate $H_2$ efficiently in saline organic wastewater. Theoretical calculations revealed that the introduction of oxygen vacancy can improve the conductivity of photoelectrode and promote the efficiency of hole and electron separation. More importantly, the activation energy of $Cl^-$ and water was reduced, and the generation of active free radicals in the photoanode system was significantly enhanced. Therefore, the $O_v$-$TiO_2$ photoanode could activate $Cl^-$ in a wide pH range (2−12), achieve degradation of 4-CP and $H_2$ generation, and greatly inhibit the production of chlorate as a by-product (the yield was only 1.04 mg $L^{-1}$). This study confirmed that the oxygen vacancy regulation strategy is an effective way to improve the treatment efficiency of pollutants in PEC-Cl system.

## 2. Materials and methods

### 2.1. Materials

The fluorine doped tin oxide (FTO) glass (20 ×30 ×2.2 mm) was purchased from South China Science & Technology Co., Ltd. $K_2TiO(C_2O_4)_2$, $Na_2CO_3$, Nitrobenzene (NB), EDTA-2Na and $NaHCO_3$ were purchased from Aladdin Industrial Corporation. $Na_2HPO_4$, $KH_2PO_4$, NaCl and $Na_2SO_4$ were purchased from Shanghai Rich Joint Chemical Reagents Co., Ltd. All chemical reagents were used as received without any further purification. Experimental water was provided by deionized water system (OKP-H120).

### 2.2. Electrode preparation and analytical methods

The specific preparation and analysis methods were stated in Supplementary material.

### 2.3. Experimental setup

An H-type double cell (200 mL) separated by a proton exchange membrane (Nafion 117) with a three-electrode system was used as the reactor (Fig. S2), which includes a counter electrode (1 ×1 $cm^2$ platinum sheet), a reference electrode (saturated calomel electrode SCE) and a working electrode (2 ×2 $cm^2$ $TiO_2$ or $O_v$-$TiO_2$). The relevant photoelectrochemical data were recorded in an electrochemical workstation (CHI660E). The PEC system mentioned in this work meant that the electrolyte contained only 0.1 M $Na_2SO_4$ while PEC-Cl contained a concentration of 50 mM NaCl and 0.1 M $Na_2SO_4$. The light source was provided by a 300 W xenon lamp light source system (CEL-HXF300-T3) with a cutoff filter (AM 1.5, 400 mW $cm^{-2}$). Pollutant degradation and $H_2$ generation reactions were carried out in anode and cathode chamber of the H-type reactor, respectively. 1 mL of the solution was taken for analysis and determination each time. In order to avoid the reaction of pollutants with RCS and FCS, no pollutant was added to the anode chamber during the determination of FCS generation. In particular, the relevant electrochemical characterization was performed with three-electrode system in a volume of 100 mL single cell containing 70 mL 0.1 M $Na_2SO_4$ solution.

### 2.4. DFT calculations

First-principles calculations under the framework of DFT were

performed in the Vienna ab-initio Simulation Package (VASP) with the version of 5.4.1. The details were presented in the Supplementary material.

## 3. Results and discussion

### 3.1. Characteristics of photoanode

The XRD patterns of $TiO_2$ and $O_v$-$TiO_2$ corresponded to the tetragonal rutile $TiO_2$ (JCPDS No.88–1175, a=b=0.4517 nm, c=0.2940 nm) (Fig. 1a). The crystallinity of $O_v$-$TiO_2$ was weakened mainly due to surface defects after electrochemical reduction, as shown by the significant decrease of (002) crystal plane peak. The surface oxygen defects were further analyzed by XPS (Fig. 1b). The binding energies of 459.1 eV (Ti $2p_{3/2}$) and 465.1 eV (Ti $2p_{1/2}$) were observed in $TiO_2$ which can be assigned to $Ti^{4+}$. For $O_v$-$TiO_2$, the both Ti 2p peaks were shifted to a lower binding energy, compared to that of $TiO_2$. This result indicates the presence of $Ti^{3+}$ in $O_v$-$TiO_2$ (Koo et al., 2017; Xu et al., 2020; Liao et al., 2014). Therefore, we also analyzed the XPS of $TiO_2$ and $O_v$-$TiO_2$ by the subtraction method and found that the peaks of $Ti^{3+}$ were presented in $O_v$-$TiO_2$, further revealing the oxygen vacancies in $O_v$-$TiO_2$. Moreover, XPS spectra of O 1 s were used to confirm the presence of oxygen vacancies too (Fig. S3), The O 1 s XPS spectra of $O_v$-$TiO_2$ were deconvoluted with three major peaks, located at 529.78, 531.06 and 531.86 eV, respectively, which could be corresponded to the lattice oxygen ($O_L$), oxygen defect ($O_V$) and chemisorbed oxygen region ($O_C$) (Lim et al., 2019; Wang et al., 2018b; Zhang et al., 2014). And the ratio of $O_V$ in the $O_v$-$TiO_2$ was 2.6 times higher than that of the $TiO_2$, indicating the formation of oxygen vacancy in the $O_v$-$TiO_2$ (Table S1). And the O/Ti ratio (2.81) of $O_v$-$TiO_2$ was much smaller than that (2.87) of $TiO_2$, further demonstrating the presence of oxygen vacancy in the $O_v$-$TiO_2$ (Table S2). Furthermore, we measured the UV–vis absorption spectra of the $TiO_2$ and $O_v$-$TiO_2$, and found that the light absorption of $O_v$-$TiO_2$ was slightly shifted from 408 nm to 413 nm (Fig. S4). Clearly, oxygen vacancies of $O_v$-$TiO_2$ could not significantly affect its light absorption properties. We believe that it can be attributed to the low content of oxygen vacancy in $O_v$-$TiO_2$ photoelectrode. And the color of $O_v$-$TiO_2$ film was slightly deepened after electrochemical reduction, which implied its light absorption would not get a big increase (Fig. S5). The similar phenomenon also exists in previous studies (Kim et al., 2018).

The morphology of $TiO_2$ and $O_v$-$TiO_2$ nanorods array electrode were characterized by FESEM and TEM (Fig. 1c-e, S6). The $O_v$-$TiO_2$ exhibited nanorod-like morphologies uniformly with an average width of about 110 nm. The interplanar spacings of 2.0 ± 0.1 Å and 3.2 ± 0.1 Å were

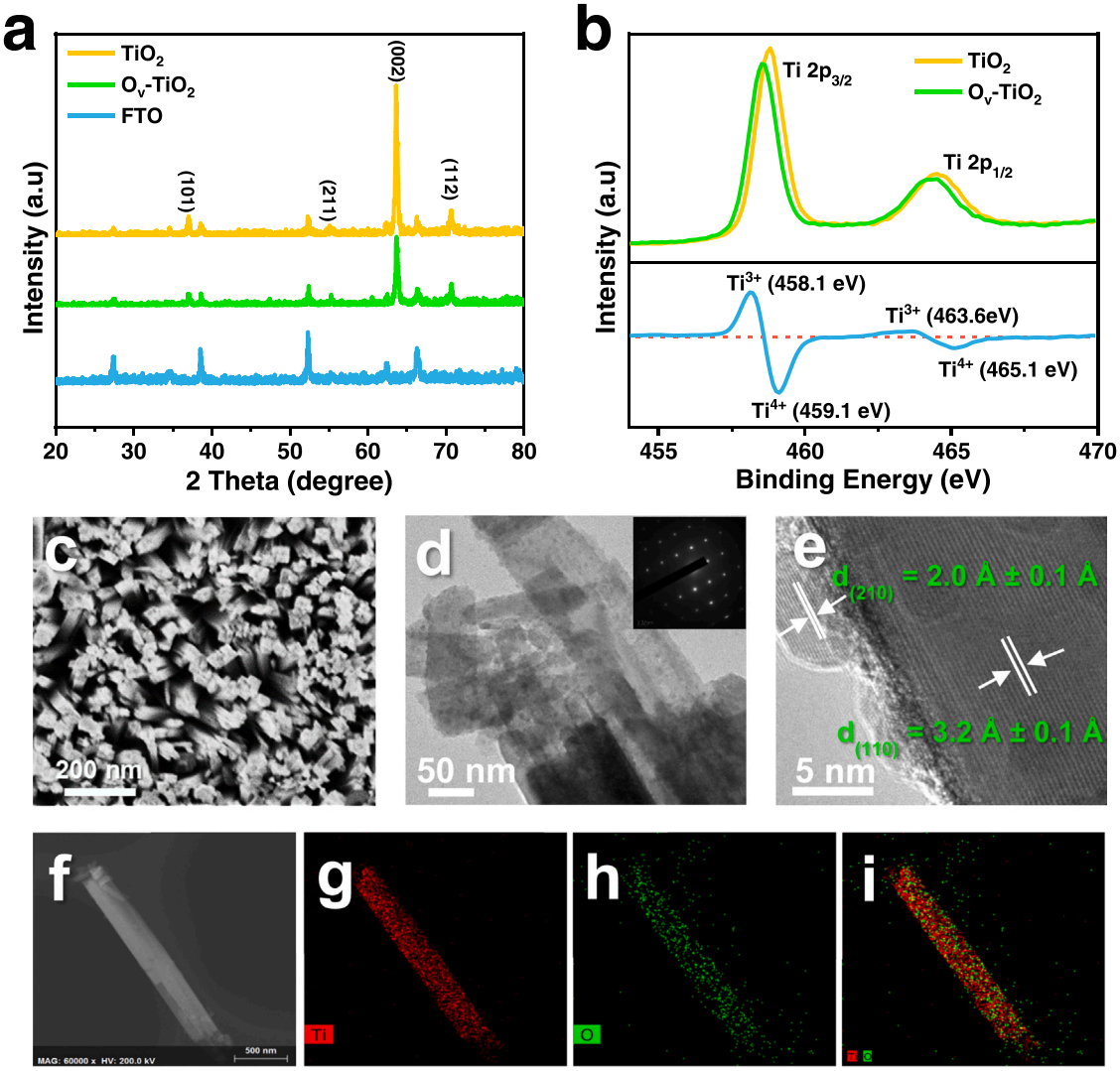


**Fig. 1.** (a) XRD patterns of FTO, $TiO_2$ and $O_v$-$TiO_2$. (b) The difference XPS spectra of Ti 2p band between $TiO_2$ and $O_v$-$TiO_2$, (c) FESEM image from the top surface view, (d) TEM image and (e) HRTEM image of $O_v$-$TiO_2$. The inset of (d) shows SAED pattern of $O_v$-$TiO_2$, (f-i) The EDS elemental mapping images of $O_v$-$TiO_2$ about Ti and O.

consistent with the (201) and (110) facet of $TiO_2$, respectively. Selected area electron diffraction (SAED) pattern was uniformly arranged, indicating the single crystal of $TiO_2$ (the inset of Fig. 1d). EDS mapping analysis showed that the Ti and O elements in the nanorods were uniformly distributed (Fig. 1f-i). This 1D single crystal $TiO_2$ nanorods array is very advantageous for the rapid transfer of electrons. In addition, the 1D nanorods array not only has a huge specific surface area, but also enhances its light absorption due to the multiple reflections of light in the array structure (Dai et al., 2020; Park et al., 2021; Li et al., 2016). The contact angle measurement showed that both $TiO_2$ and $O_v$-$TiO_2$ electrodes had strong hydrophilicity (Fig. S7), which could promote the contact of pollutants and $Cl^-$ in wastewater to the electrode surface, thus accelerating the PEC chlorine activation and pollutants degradation reactions.

### 3.2. Effects of oxygen vacancies content on $TiO_2$ photoanode

The oxygen vacancies-enriched $TiO_2$ photoanode was successfully prepared by electrochemical reduction technology. The content of oxygen vacancies was regulated by controlling the time of electrochemical reduction. As shown in Fig. S5, the color of $TiO_2$ photoelectrode gradually deepened with the extension of electrochemical reduction time, which is the characteristic of the increase of oxygen vacancy concentration(Kim et al., 2018, Koo et al., 2017). Furthermore, we carried out photocurrent responses measurement to investigate influence of the content of oxygen vacancies on the PEC-Cl performance, and $Cl^-$ activation experiment (Fig. S8). The results showed that the appropriate content of oxygen vacancy (electrochemical reduction by 180 s) could improve the carrier separation efficiency and the photocurrent response, promoting the activation of $Cl^-$ to generate more FCS.

### 3.3. Photoelectrochemical degradation and $H_2$ generation performance

The degradation of 4-CP coupled with $H_2$ generation on $O_v$-$TiO_2$ were compared with $TiO_2$ in electroncatalysis (EC), photocatalysis (PC), PEC and PEC-Cl systems (Fig. 2a, b). The results showed that the $TiO_2$ and $O_v$-$TiO_2$ exhibited no obvious degradation of 20 ppm 4-CP, and $H_2$ production in EC and PC systems. However, in PEC systems, the degradation rate of 4-CP within 60 min was 31.7% by $O_v$-$TiO_2$, which is higher than that on $TiO_2$ (18.0%). Furthermore, the $H_2$ generation rate on $O_v$-$TiO_2$ was 161.3 μmol $h^{-1}$ $cm^{-2}$, which is 8.6 times higher than that of $TiO_2$.

Interestingly, in PEC-Cl systems, both the degradation rate of 4-CP within 60 min on $O_v$-$TiO_2$ and $TiO_2$ were increased so much. It reached 99.9% on $O_v$-$TiO_2$, while that was 33.1% for $TiO_2$. In addition, the $H_2$ generation rate of $O_v$-$TiO_2$ was also as high as 198.2 μmol $h^{-1}$ $cm^{-2}$, which is about 7.2 times higher than that of $TiO_2$ and also higher than that on $O_v$-$TiO_2$ without $Cl^-$. $O_2$ was not detected in the PEC-Cl system (Fig. S9). These results indicate that $O_v$-$TiO_2$ had much more excellent photoelectrochemical performance than $TiO_2$ in pollutants degradation and $H_2$ generation. Meanwhile, it was verified that overall catalytic performance of the PEC-Cl system on whatever the $TiO_2$ or $O_v$-$TiO_2$ was better than that in the PEC system, revealing the important role of $Cl^-$ in the PEC-Cl system. Furthermore, similar results were also obtained in the degradation of Phenol and Bisphenol A (BPA) in the PEC-Cl system with $O_v$-$TiO_2$ (Fig. S10). In the PC and EC systems, the degradation of Phenol and BPA and $H_2$ generation rate was not worth mentioning. The removal rate of 20 ppm Phenol within 60 min was 31.7% and $H_2$ generation rate was 163.7 μmol $h^{-1}$ $cm^{-2}$ in the PEC system. The removal rate of 20 ppm BPA within 60 min was 39.2% and $H_2$ generation rate was 160.7 μmol $h^{-1}$ $cm^{-2}$ in the PEC system. For the PEC-Cl system, 99.9% Phenol can be removed within 30 min and the $H_2$ generation rate was 195.6 μmol $h^{-1}$ $cm^{-2}$. And 99.9% BPA can be removed within 30 min and the $H_2$ generation rate was 192.5 μmol $h^{-1}$ $cm^{-2}$. These results further proved that the PEC-Cl system with $O_v$-$TiO_2$ photoanode possesses excellent POPs degradation and $H_2$ generation performance compared with PEC-Cl and PEC systems reported in recent years (Table S3).

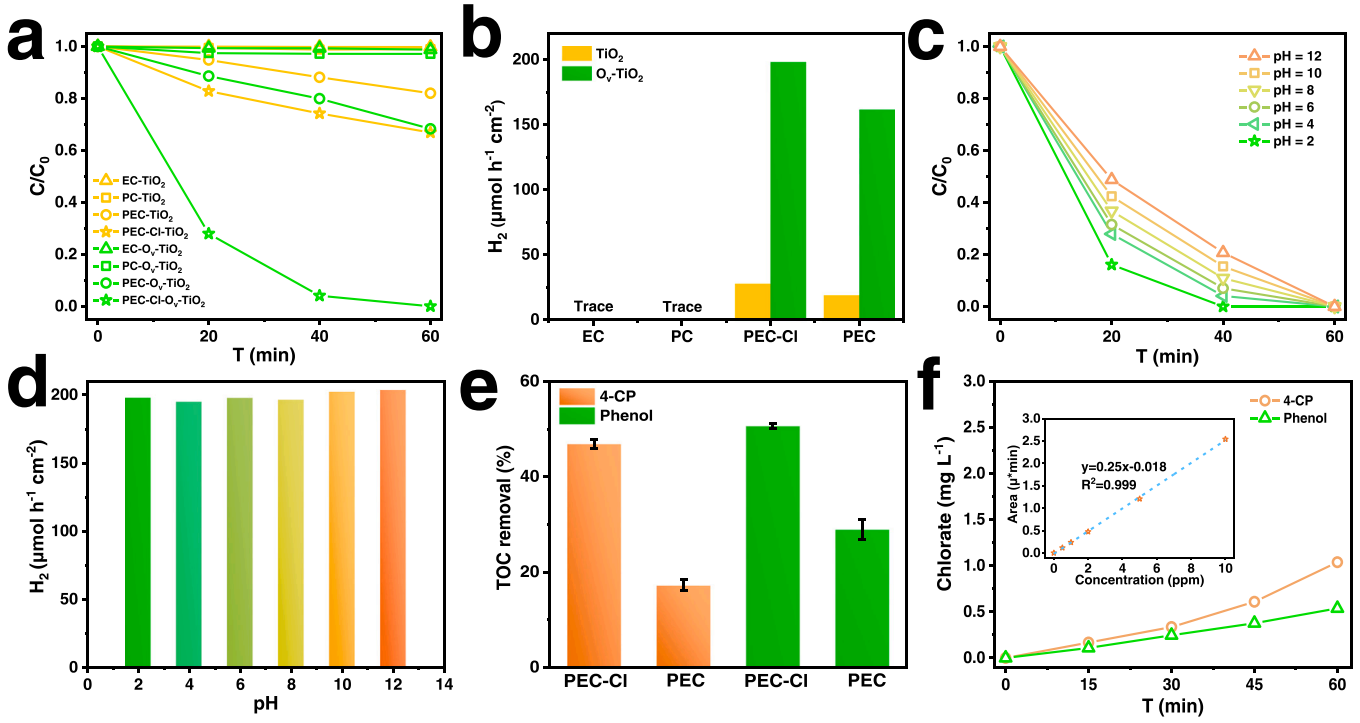


**Fig. 2.** (a) The degradation of 4-CP and (b) the generation rate of $H_2$ on $TiO_2$ (yellow lines) and $O_v$-$TiO_2$ (green lines) in PC, EC, PEC and PEC-Cl systems. (c) The degradation of 4-CP and (d) the generation rate of $H_2$ on $O_v$-$TiO_2$ in PEC-Cl system under different pH, (e) TOC removal efficiency of 4-CP and Phenol on $O_v$-$TiO_2$ in PEC and PEC-Cl system after 180 min reaction, (f) the concentrations of chlorate on $O_v$-$TiO_2$ in the PEC-Cl system. The inset of (f) is standard curve of chlorate concentration. ($[4\text{-CP}]_0$ = 20 ppm, [NaCl] = 50 mM, $[Na_2SO_4]$ = 0.1 M, + 0.5 V (vs. SCE), pH = 4, simulated sunlight irradiation.).

To better clarify the performance of the PEC-Cl system with $O_v$-$TiO_2$ photoanode, we further investigated the degradation of POPs and $H_2$ generation performance under different pH (Fig. 2c, d), bias voltage (Fig. S11a, b) and chlorine ions concentration (Fig. S11c, d). We found that 99.9% of 20 ppm 4-CP could be efficiently removed within 60 min in a pH range of 2–12, and the generating $H_2$ rate remained at an extremely high level (around 200 μmol $h^{-1}$ $cm^{-2}$). Moreover, we determined the concentration of FCS generated by the PEC-Cl system under different pH conditions, and found that the concentration of FCS generated under acidic conditions was slightly higher than that of alkaline condition (Fig. S12). This result indicated that the degradation efficiency could be affect by pH value due to the low FCS yield. The results show that the PEC-Cl system with $O_v$-$TiO_2$ photoanode has wide pH adaptability and enables pollutants degradation and $H_2$ generation under extreme conditions. The effect of bias voltage on pollutants degradation and $H_2$ generation was investigated in the voltage range of 0–1.0 V (vs. SCE). As the applied bias voltage increased from 0 V to 1.0 V, the degradation of 4-CP and the $H_2$ generation rate were significantly promoted in PEC-Cl system (Fig. S11a, b). That may indicate the bias voltage can accelerate the separation of carriers resulting in a large number of holes to degrade the pollutant and electrons to generate $H_2$. As for the chlorine ions concentration effect, the $H_2$ generation rate and 4-CP removal rate gradually increased with the increasing of the concentration from 0 to 100 mM (Fig. S11c, d). With high concentration of $Cl^-$, its activation by holes was promoted which not only inhibited the recombination of photo-generated carriers, but also enhanced the formation of RCS and accelerated the $H_2$ generation and pollutant degradation. Above all, these results reveal that the PEC-Cl system with $O_v$-$TiO_2$ photoanode can be applied to purify the wastewater under complex conditions.

Total organic carbon (TOC) removal rate of POPs was also measured and compared for PEC and PEC-Cl system with $O_v$-$TiO_2$ photoanode (Fig. 2e). After 180 min of photoelectrochemical reaction in the PEC system, the TOC removal rates of Phenol and 4-CP were only 17.2% and 28.9%, respectively. However, in the PEC-Cl system, the TOC removal rates of Phenol and 4-CP were increased to 50.6% and 46.9%, respectively. These results indicate that the presence of $Cl^-$ remarkably strengthened the TOC removal efficiency in the PEC-Cl system, which is consistent with the result of the degradation of pollutants in PEC-Cl system. It is generally recognized that some molecular organic matter could be produced in the photoelectrochemical degradation of 4-CP. Meanwhile, the degradation rate of contaminant could be not consistent with the mineralization rate (Song et al., 2021; Koo et al., 2019; Lim et al., 2019). Therefore, we extended the reaction time to 10 h, and found that the TOC removal efficiency of 4-CP was over 91% in the PEC-Cl system (Fig. S13). This indicated that PEC-Cl degradation of 4-CP using $O_v$-$TiO_2$ photoelectrode could not produce secondary pollution. In addition, the concentrations of toxic by-product chlorate during the degradation of Phenol and 4-CP in the PEC-Cl system with 50 mM NaCl were also monitored by IC. As shown in Fig. 2f, the concentration of chlorate gradually increases with time. However, when Phenol and 4-CP were completely degraded, the concentrations of chlorate were only

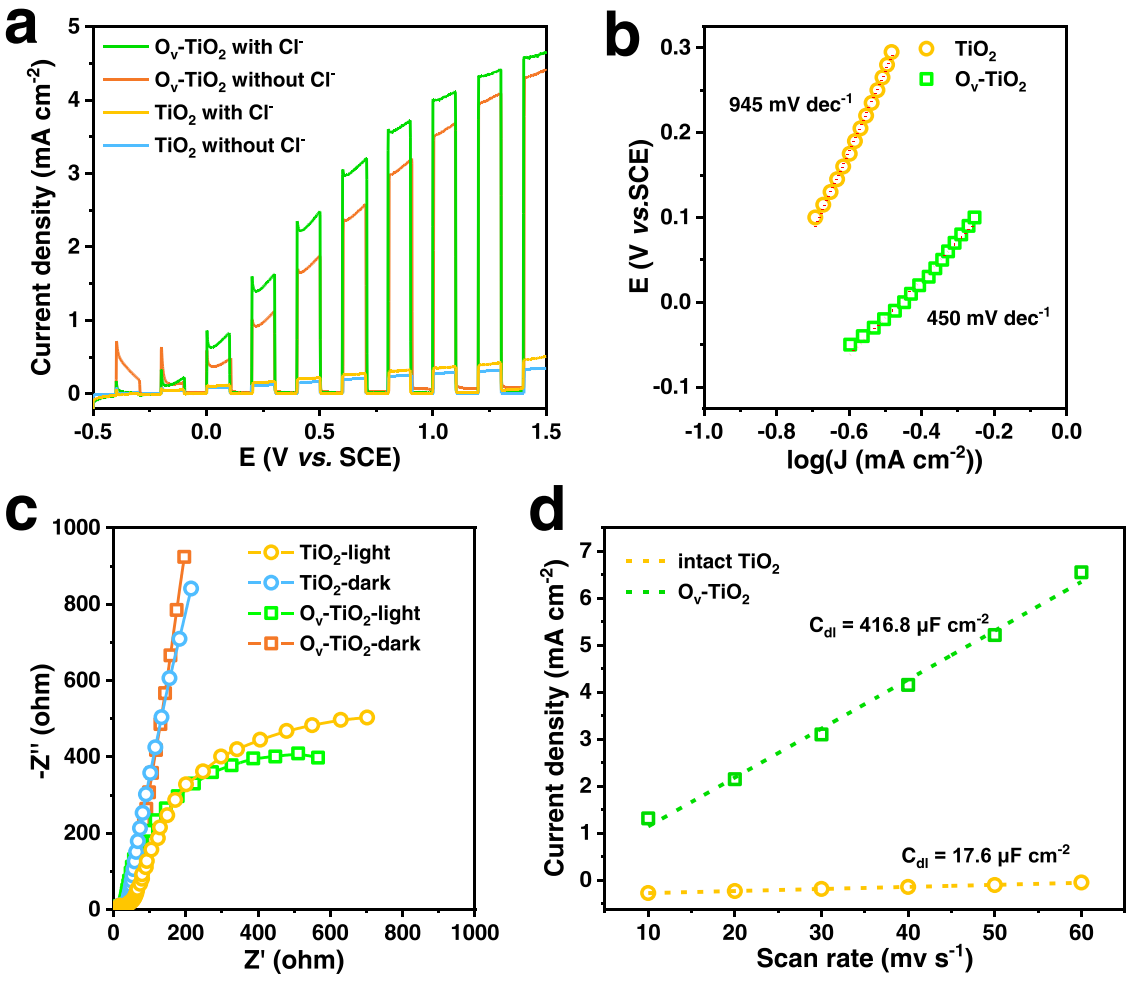


**Fig. 3.** (a) The discontinuous linear sweep voltammetry of $TiO_2$ and $O_v$-$TiO_2$ with or without 50 mM NaCl under simulated solar light irradiation, (b) Tafel slopes fitted from a continuous LSV under simulated sunlight irradiation, (c) the electrochemical impedance spectroscopy under simulated sunlight irradiation or dark, (d) the electrochemical double-layer capacitance of $TiO_2$ and $O_v$-$TiO_2$.

1.04 mg $L^{-1}$ and 0.53 mg $L^{-1}$, respectively, which are an extremely low, non-toxic, dischargeable concentration (Hou et al., 2018; Zhang et al., 2021). These results suggest that the PEC-Cl system with $O_v$-$TiO_2$ is an environmentally friendly catalytic system and very suitable for industrial saline organic wastewater treatment.

### 3.4. Photoelectrochemical performance measurement

The intrinsic photoelectrochemical properties of $TiO_2$ and $O_v$-$TiO_2$ were investigated to understand the high PEC activity of the $O_v$-$TiO_2$ photoanode. As shown in Fig. 3a, the photocurrent response intensities of $O_v$-$TiO_2$ were much higher than those of $TiO_2$ whatever with or without $Cl^-$ under light irradiation. As for $O_v$-$TiO_2$, $Cl^-$ would slightly enhance the photocurrent, suggesting that the $Cl^-$ can promote the separation of photogenerated carriers in the chlorine-containing PEC system. The corresponding electrochemical kinetic Tafel slopes were obtained by fitting the continuous LSV curves (Fig. S14a). The Tafel slope of $O_v$-$TiO_2$ was 450 mV $dec^{-1}$, which is much smaller than that of $TiO_2$ (945 mV $dec^{-1}$) (Fig. 3b). This result indicates that $O_v$-$TiO_2$ possessed a faster electron transfer rate than the $TiO_2$. Moreover, $O_v$-$TiO_2$ could undergo the PEC reaction with a lower over-potential at the same current density. The electrochemical impedance spectra showed that the Nyquist curves of $TiO_2$ and $O_v$-$TiO_2$ were linear transport model under dark condition, indicating that there would be large resistance for the charge transfer (Fig. 3c). Under the sunlight irradiation, obvious semicircular models were observed on both $TiO_2$ and $O_v$-$TiO_2$. The impedance arc radius of $O_v$-$TiO_2$ was slightly smaller than that of $TiO_2$, indicating that $O_v$-$TiO_2$ was more conducive to the electron transfer.

The Mott-Schottky curves of $TiO_2$ and $O_v$-$TiO_2$ were measured at frequencies of 500, 1000, and 1500 Hz. As shown in Fig. S14b and c, the Mott-Schottky curves of $O_v$-$TiO_2$ had much smaller slopes than the $TiO_2$. Photogenerated carrier densities ($N_D$) at 500 Hz can be calculated according to the follow equation:

$$N_D = \frac{2}{e\varepsilon\varepsilon_0}\frac{dE}{d(\frac{1}{C^2})}$$

where $N_D$ reflects the photogenerated carriers density, $e$ refers to the charge value, $\varepsilon_0$ is the vacuum permittivity, $\varepsilon$ is the semiconductor permittivity, $E$ is the applied potential, and $C$ represents the space charge capacitance (Xiao et al., 2019). The $N_D$ of $O_v$-$TiO_2$ was $9.38 \times 10^{23}$ $cm^{-3}$, much larger than the $TiO_2$ ($5.64 \times 10^{21}$ $cm^{-3}$). This is only a qualitative analysis since the value of $N_D$ was calculated from the flat-electrode model. This result suggests that oxygen vacancies significantly increase the electrical conductivity of photoelectrode and then facilitate the electron transfer. Transient photocurrents were also measured under the same condition (Fig. S8a). The average photocurrent response value of $O_v$-$TiO_2$ reached to 2.4 mA $cm^{-2}$ with good cyclic stability, which is much higher than that of 0.4 mA $cm^{-2}$ for $TiO_2$. This result further confirms the excellent PEC performance of $O_v$-$TiO_2$. In

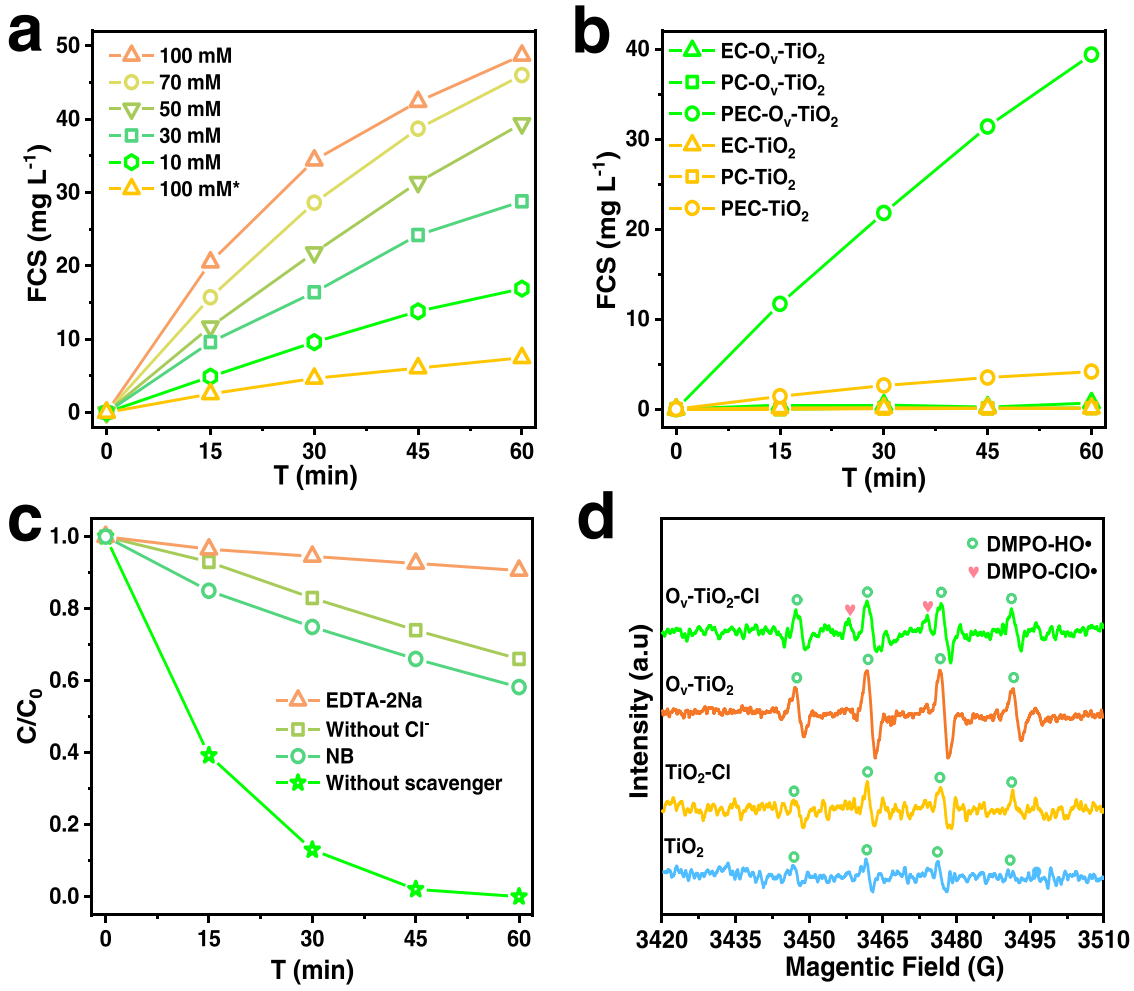


**Fig. 4.** (a) The generation of FCS on $O_v$-$TiO_2$ with different chlorine concentrations (100 mM* refers to the $TiO_2$ with 100 mM chlorine concentration), (b) the generation of FCS on both $TiO_2$ and $O_v$-$TiO_2$ in PC, EC and PEC conditions, (c) the degradation of 4-CP on $O_v$-$TiO_2$ in PEC-Cl system in the presnece of various scavengers, (d) EPR spectra of $TiO_2$ and $O_v$-$TiO_2$ in PEC and PEC-Cl systems ($[4\text{-CP}]_0$ = 20 ppm, [NaCl] = 50 mM, $[Na_2SO_4]$ = 0.1 M, + 0.5 V (vs. SCE), pH = 4, simulated solar-light irradiation).

addition, the CV curves of $TiO_2$ and $O_v$-$TiO_2$ were measured with different scanning speeds (Fig. S15), their electrochemical surface area (ECSA) were estimated by the electrochemical double-layer capacitance method (Fig. 3d). The ECSA of $O_v$-$TiO_2$ (416.8 μF $cm^{-2}$) is 23 times of that of $TiO_2$ (17.6 μF $cm^{-2}$). Based on the above analysis, the increased removal efficiency of 4-CP and $H_2$ generation on $O_v$-$TiO_2$ in PEC-chlorine system may be attributed to its much more efficient photogenerated charge carrier separation efficiency compared to the $TiO_2$.

### 3.5. Mechanism of chlorine activation and degradation of pollutants

To investigate the significant role of $Cl^-$ in the catalytic system, the generation of free chlorine species (FCS) on $TiO_2$ and $O_v$-$TiO_2$ was measured with different $Cl^-$ concentrations (Fig. 4a). To exclude the effect of $H_2O_2$, we performed a controlled experiment without $Cl^-$ (Fig. S16). The absorbance of the reacted solution had no change with DPD during the reaction, demonstrating that the determination of FCS by DPD coloration method could not be affected by $H_2O_2$. It should be noted that FCS were converted from chlorine radical species (Koo et al., 2019). As the $Cl^-$ concentration increased from 10 to 100 mM in PEC-Cl system, the FCS generated by $O_v$-$TiO_2$ also increased from 16.9 to 48.7 mg $L^{-1}$. In addition, the accumulation of FCS increased gradually with time in PEC-Cl system with whatever the $TiO_2$ or $O_v$-$TiO_2$ photoanodes. In the PEC-Cl system with 100 mM chlorine concentration, the generation of FCS was 48.7 mg $L^{-1}$ by $O_v$-$TiO_2$ within 60 min, which is about 6.5 times than that with $TiO_2$ (7.5 mg $L^{-1}$). The results clearly demonstrate that $O_v$-$TiO_2$ can generate more RCS than $TiO_2$ by activating $Cl^-$ at the same condition, which greatly promotes the degradation of POPs. Moreover, the generation of FCS by $O_v$-$TiO_2$ and $TiO_2$ were compared under variable energy input conditions (PEC, PC, and EC) with 50 mM chlorine concentration. Fig. 4b shows that FCS was only observed in PEC condition. That may be caused by the poor separation efficiency of photogenerated carriers in the PC condition without bias voltage and the not enough voltage required for $Cl^-$ activation (1.36 V vs. NHE) in the EC condition (+ 0.5 V vs. SCE) (Koo et al., 2019). This implies that the synergy effect of bias voltage and sunlight in PEC system leads to the generation of RCS, and thus the degradation of pollutants.

To further clarify the main activated oxidants produced by $O_v$-$TiO_2$, EDTA-2Na and NB were used to scavenge holes and •OH radicals in the PEC-Cl degradation of 4-CP, and the PEC system without $Cl^-$ were set as a blank control (Fig. 4c). In the presence of EDTA-2Na, the degradation of 4-CP was completely inhibited, which indicates that the degradation of pollutions was triggered by holes. The degradation rate of 4-CP was 41.8% due to •OH radicals were scavenged in PEC-Cl system. This is mainly attributed to holes and RCS. Moreover, we found that the degradation rate of 4-CP in the PEC system without $Cl^-$ was only 34.0%, which is mainly caused by holes and •OH radicals. However, the degradation rate of 4-CP was 99.9% in the PEC-Cl system with $Cl^-$, which is attributed to the synergy of the holes, RCS and •OH. The above results clearly reveal that the photogenerated holes were the fundamental oxidants for the degradation of pollutants, having the ability to activate $H_2O$ and $Cl^-$ which also was demonstrated in previous reports (Song et al., 2021; Kim et al., 2018; Li et al., 2021c). And the effect of RCS was significantly greater than •OH free radicals. Meanwhile, we used EPR spin-trapping technique to explore the working mechanism of the PEC-Cl system (Fig. 4d). The signal peak of DMPO-•OH with 1:2:2:1 intensity was observed in PEC and PEC-Cl system, indicating the existence of •OH radical. However, the signal intensity of •OH radical on $O_v$-$TiO_2$ was stronger than that on $TiO_2$ in PEC system. Moreover, in the PEC-Cl system, ClO• radical signal peak on $O_v$-$TiO_2$ was clearly observed, which was negligible on $TiO_2$. In addition, in the systems with $O_v$-$TiO_2$ photoanode, the signal intensity of •OH radical in PEC system was significantly higher than that in PEC-Cl system. However, the signal intensity of •OH radical was weak and the distinction was insignificant for $TiO_2$ photoanode. This might be due to the •OH reacted with FCS (such as HClO/ $ClO^-$) for the formation of ClO• radical. The EPR results also demonstrated that no $SO_4$•$^-$ was produced in PEC and PEC-Cl system (Fig. 4d). No $S_2O_8^{2-}$ was detected by ion chromatography (IC) (Fig. S17). This may because the low bias, which was applied in our reaction system, favors the activation of $Cl^-$ and $H_2O$, but disfavors the activation of $SO_4^{2-}$. These results indicate that $O_v$-$TiO_2$ significantly enhanced the generation of •OH in PEC system and promote the formation of RCS in PEC-Cl system. This further explains that the PEC-Cl system with $O_v$-$TiO_2$ photoanode possesses a better degradation performance of POPs.

In order to better understand the reasons for the excellent photoelectrochemical degradation activity of the catalysts, the DFT calculation was performed to study on the adsorption of $H_2O$ and $Cl^-$, and the further oxidation to •OH and Cl• on $TiO_2$ and $O_v$-$TiO_2$. The specific details of DFT theoretical calculation models were shown in Fig. S18. As shown in Fig. 5a, chloride ions were adsorbed on $O_v$-$TiO_2$ with the adsorption energy of − 0.14 eV, which is 7 times larger than that of $TiO_2$. Furthermore, the rate-determining step of $Cl^-$ activation, $*Cl^- + h^+ = *Cl$, was spontaneous with a Gibbs free energy of − 0.47 eV on $O_v$-$TiO_2$, while that was 1.28 eV on the $TiO_2$. It indicates that $O_v$-$TiO_2$ had better $Cl^-$ adsorption and activation performance than $TiO_2$, which is consistent with the results of chlorine activation experiments in PEC-Cl system. As shown in Fig. 5b, the adsorption energy of $H_2O$ on $TiO_2$ and $O_v$-$TiO_2$ was − 0.77 eV and − 0.41 eV, respectively. $*OH^- + h^+ = *OH$ is the rate-determining step of $H_2O$ activation and its energy barrier was 2.19 eV on $TiO_2$, which is much higher than that of 0.49 eV on $O_v$-$TiO_2$. It suggests that $O_v$-$TiO_2$ had a better performance of $H_2O$ activation to form •OH radicals than $TiO_2$, which is also consistent with the results of EPR experiments. Meanwhile, the reaction process was calculated under light irradiation, and the U value was modified to 2.79 eV for $TiO_2$ and 2.66 eV for $O_v$-$TiO_2$. As shown in Fig. S19, the calculation results also indicate that $O_v$-$TiO_2$ had better $Cl^-$ and $H_2O$ activation performance than $TiO_2$ under light irradiation. These results further explain the efficient degradation ability of the PEC-Cl system by using $O_v$-$TiO_2$ photoanode.

Based on the above experimental and theoretical calculation results, we proposed the $Cl^-$ activation and organic pollutants degradation mechanism in the industrial saline organic wastewater on the $O_v$-$TiO_2$ as shown in Fig. 5c. The main reaction steps were as follows (Li et al., 2020; Koo et al., 2019; Zhang et al., 2021; Li et al., 2021d; Zhang et al., 2018; Shao et al., 2022):

$$O_v\text{-}TiO_2 + hv \rightarrow h^+ + e^- \quad (1)$$

$$H_2O + h^+ \rightarrow H^+ + \bullet OH \quad (2)$$

$$Cl^- + h^+ \rightarrow Cl\bullet \quad (3)$$

$$Cl\bullet + Cl\bullet \rightarrow Cl_2 \quad (4)$$

$$Cl_2 + H_2O \rightarrow HClO + HCl \quad (5)$$

$$Cl\bullet + HClO \rightarrow ClO\bullet + HCl \quad (6)$$

$$\bullet OH + HClO \rightarrow ClO\bullet + H_2O \quad (7)$$

$$\bullet OH + ClO^- \rightarrow ClO\bullet + OH^- \quad (8)$$

$$\bullet OH \,/\, ClO\bullet + Org\cdot \rightarrow CO_2 + H_2O + Cl^- \quad (9)$$

$O_v$-$TiO_2$ generates $e^-$ and $h^+$ pairs under light irradiation, and the $e^-$ is exported to the cathode through the external circuit for reducing $H^+$ and generating $H_2$. The abundant $h^+$ left on the surface of $O_v$-$TiO_2$ quickly reacts with $H_2O$ and $Cl^-$ to generate •OH and Cl• radicals. The combination of the two Cl• radicals can form $Cl_2$, which can react with $H_2O$ to form HClO. And then, the •OH and Cl• radicals react with HClO to form ClO• radicals with strong oxidizing ability. Active oxide species such as $h^+$, •OH and RCS in the reaction system react with electron-rich POPs to mineralize them into $CO_2$ and $H_2O$, achieving the goal of purifying the water environment.

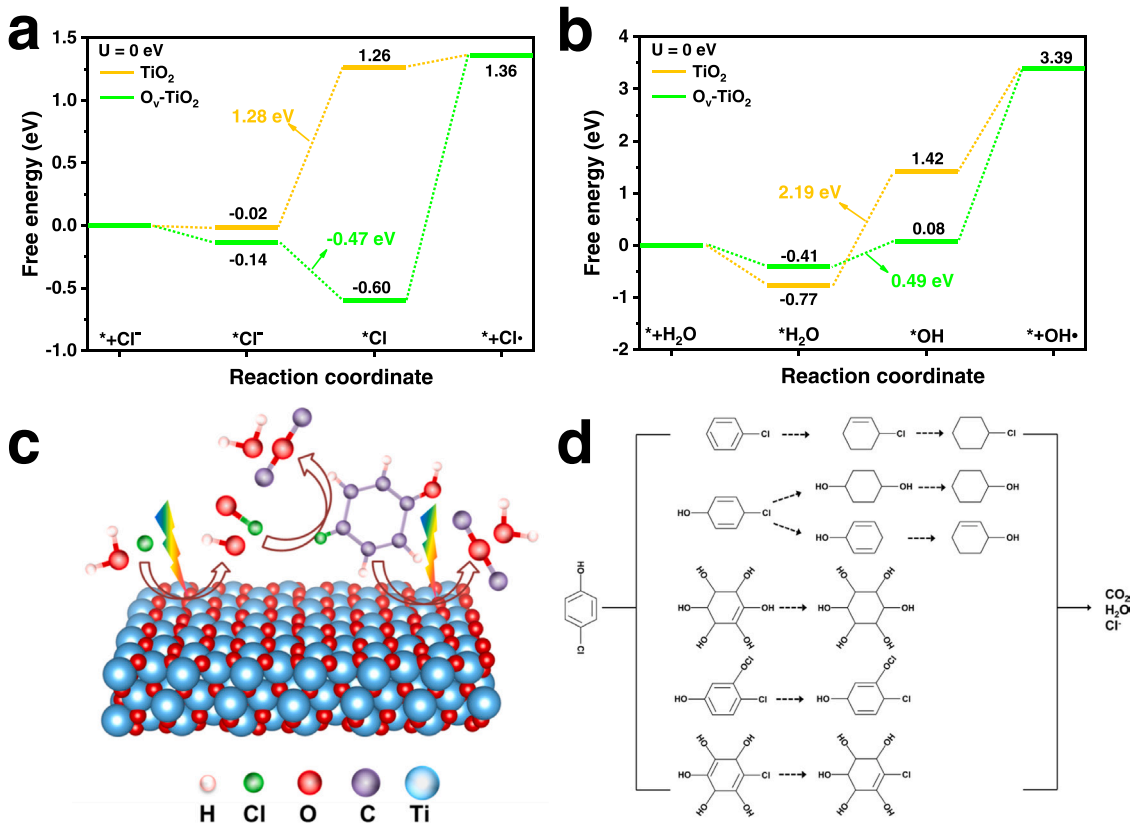


**Fig. 5.** The Gibbs free energy diagrams about the formation of (a) Cl• and (b) •OH on $TiO_2$ and $O_v$-$TiO_2$, (c) the degradation scheme of 4-CP by active species on $O_v$-$TiO_2$, (d) Degradation pathways for 4-CP in PEC-Cl system.

Besides, we applied LC-MS to analyze possible intermediates in the process of 4-CP degradation. Some major intermediates were observed and their possible molecular structures were shown in Fig. S20. Typically, these products were produced through a series of processes such as oxidation, ring opening and fragmentation. Ideally, these products would eventually mineralize into $CO_2$ and $H_2O$. The possible degradation pathways of 4-CP in the PEC-Cl system were illustrated in Fig. 5d.

### 3.6. Electrical energy consumption and stability of the PEC-Cl system

The performance and electrical energy consumption of the EC and PEC active chlorine systems with $O_v$-$TiO_2$ photoanode were also studied. As shown in Fig. 6a, the degradation efficiency of 4-CP and $H_2$ generation rate gradually increased with the increase of voltage. This may be due to the generation rate of RCS from $Cl^-$ accelerated under high bias voltage conditions. However, in EC active chlorine system, even when the bias voltage was at 3.0 V, the $H_2$ generation rate was 171.6 μmol $h^{-1}$ $cm^{-2}$ and the degradation rate of 4-CP was 60% within 60 min, which are far inferior to the performance of PEC-Cl system (198.0 μmol $h^{-1}$ $cm^{-2}$ and 99.9% within 60 min) at the low voltage of 0.5 V. In addition, assuming that the simulated sunlight of PEC system is provided by natural light sources, we monitored the current density of different active chlorine systems (Fig. S21) and estimated their electrical energy consumption in 60 min period (Table S4). The EC system at a voltage of 3.0 V consumed 90.7 J in 60 min, which is much higher than that of 0.023 J for the PEC system at voltage of 0.5 V. The degradation with $H_2$ generation experiments were also carried out under the standard of a sun (100 mW $cm^{-2}$). As shown in Fig. S22, the degradation rate of

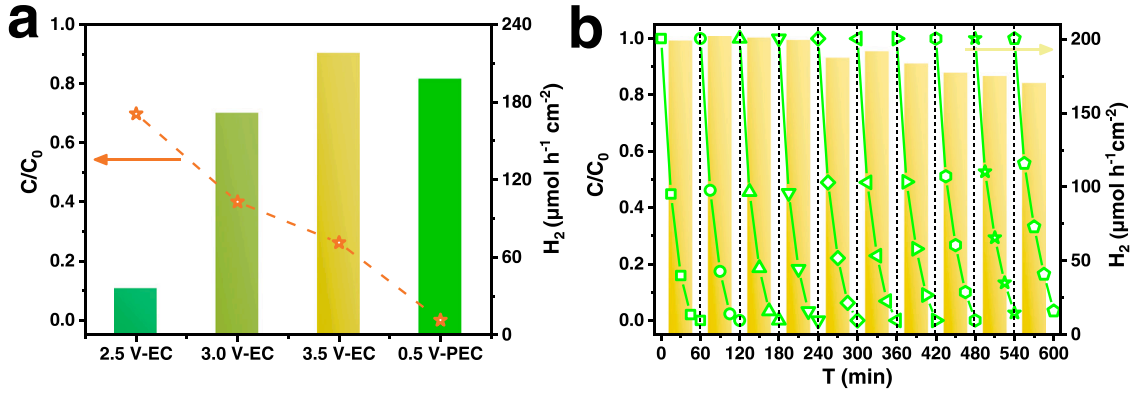


**Fig. 6.** (a) The performance for degrading 4-CP and simultaneous $H_2$ generation rate by using $O_v$-$TiO_2$ as working electrodes in both EC-Cl system and PEC-Cl systems, (b) the stability of PEC-Cl system by using $O_v$-$TiO_2$ as photoanode ($[4\text{-CP}]_0$ = 20 ppm, [NaCl] = 50 mM, $[Na_2SO_4]$ = 0.1 M, + 0.5 V (vs. SCE), pH = 4, simulated sunlight irradiation).

20 ppm 4-CP was 98.0% in 120 min, which indicated that the PEC-Cl system can also be operated efficiently under actual natural sunlight irradiation. These results show that the PEC system can effectively utilize solar energy and reduce the consumption of electricity. Furthermore, the stability of PEC-Cl system with $O_v$-$TiO_2$ photoanode was investigated (Fig. 6b). After 10 cycles, the degradation rate of 20 ppm 4-CP was still higher than 96% within 60 min and the $H_2$ generation rate still remained above 170 μmol $h^{-1}$ $cm^{-2}$. In addition, SEM (Fig. S23) and XRD (Fig. S24) were used to characterize the $O_v$-$TiO_2$ photoelectrode after the reaction, and the results showed that the crystal structure and morphology were remain stable. The inset in Fig. S23 b showed the photo of $O_v$-$TiO_2$ photoelectrode after the reaction, which was is good evidence that the $O_v$-$TiO_2$ does not peel off. It indicates that the PEC-Cl system had commendable durability suggesting its potential for practical applications in water pollution treatment.

## 4. Conclusions

Effective wastewater treatment and recycling is an ideal method to solve energy and environment issues. Appropriate technologies are required for different types of wastewater. Regarding saline organic wastewater, the treating efficiency of traditional methods is seriously affected by the poor and complex water quality. PEC, as an emerging technology, has unique advantages. The various salts in wastewater are utilized as electrolyte, and a large amount of $Cl^-$ provide chlorine source as active chlorine co-processing technology, avoiding additional substance consumption. The photoelectrode is composed of immobilized catalysts, which is easy to be separated and recycled compared with the photocatalysis technology. Furthermore, the PEC technology can generate considerable solar fuel accompanying with the purification of the wastewater, and the electricity consumed is far less than that for electrocatalysis technology. In this work, both experimental and theoretical studies have shown that the PEC-Cl system with $O_v$-$TiO_2$ photoanode possess powerful degradation and solar fuel production capabilities. In addition, the low by-product concentration also has very little impact on the environment. Besides, although the proposed PEC-Cl system in this work has very good results in the experimental stage, the further researches are still needed to developed, including increasing the size of the photoelectrode and reactor prior to its application in practical wastewater treatment.

## Environmental Implication

Effective wastewater treatment and recycling is an ideal method to solve energy and environment issues. In this work, we developed a stable and reliable PEC-Cl system to treat polluted water in an efficient, energy-saving, and environmentally friendly way. The as-designed PEC-Cl system rapidly activated $Cl^-$ to drive the deep mineralization of POPs wastewater in a wide pH range (2−12) with simultaneous production of $H_2$. It can make efficient use of solar energy and reduce the consumption of electricity. Moreover, nearly no toxic by-product of chlorates was produced during this system.

## CRediT authorship contribution statement

**Jiabao Wu:** Investigation, Experiment, Data curation, Writing – original draft. **Ying Tao:** Investigation, Experiment, Data curation, Writing – original draft. **Chi Zhang:** Overall revision. **Qiong Zhu:** Investigation. **Dieqing Zhang:** Conceptualization, Supervision, Project administration. **Guisheng Li:** Conceptualization, Supervision, Project administration, Funding acquisition, Writing – review & editing.

## Declaration of Competing Interest

The authors declare that they have no known competing financial interests or personal relationships that could have appeared to influence the work reported in this paper.

## Data Availability

Data will be made available on request.

## Acknowledgements

This work was supported by the National Key Research and Development Program of China (2020YFA0211004), National Natural Science Foundation of China (21876113, 22176127, 22022608, 21261140333), the Shanghai Engineering Research Center of Green Energy Chemical Engineering, and “111” Innovation and Talent Recruitment Base on Photochemical and Energy Materials (D18020).

## Appendix A. Supporting information

Supplementary data associated with this article can be found in the online version at doi:10.1016/j.jhazmat.2022.130363.

## References

Bilal, M., Lam, S.S., Iqbal, H.M.N., 2022. Biocatalytic remediation of pharmaceutically active micropollutants for environmental sustainability. Environ. Pollut. 293, 118582.
Chen, W., Gu, Z., Ran, G., Li, Q., 2021a. Application of membrane separation technology in the treatment of leachate in China: a review. Waste Manag 121, 127–140.
Chen, X., Huo, X., Liu, J., Wang, Y., Werth, C.J., Strathmann, T.J., 2017. Exploring beyond palladium: catalytic reduction of aqueous oxyanion pollutants with alternative platinum group metals and new mechanistic implications. Chem. Eng. J. 313, 745–752.
Chen, Y., Tong, S., Li, W., Liu, Y., Tan, F., Ge, M., Xie, X., Sun, J., 2021b. Photocatalytic oxidation of $SO_2$ by $TiO_2$: Aerosol formation and the key role of gaseous reactive oxygen species. Environ. Sci. Technol. 55 (14), 9784–9793.
Cheng, Z., Ling, L., Wu, Z., Fang, J., Westerhoff, P., Shang, C., 2020. Novel visible light-driven photocatalytic chlorine activation process for carbamazepine degradation in drinking water. Environ. Sci. Technol. 54 (18), 11584–11593.
Coates, J.D., Achenbach, L.A., 2004. Microbial perchlorate reduction: rocket-fueled metabolism. Nat. Rev. Microbiol. 2 (7), 569–580.
Dai, W., Tao, Y., Zou, H., Xiao, S., Li, G., Zhang, D., Li, H., 2020. Gas-phase photoelectrocatalytic oxidation of NO via $TiO_2$ nanorod array/FTO photoanodes. Environ. Sci. Technol. 54 (9), 5902–5912.
Frank, B.P., Smith, C., Caudill, E.R., Lankone, R.S., Carlin, K., Benware, S., Pedersen, J. A., Fairbrother, D.H., 2021. Biodegradation of functionalized nanocellulose. Environ. Sci. Technol. 55 (15), 10744–10757.
Hou, S., Ling, L., Dionysiou, D.D., Wang, Y., Huang, J., Guo, K., Li, X., Fang, J., 2018. Chlorate formation mechanism in the presence of sulfate radical, chloride, bromide and natural organic matter. Environ. Sci. Technol. 52 (11), 6317–6325.
Jassby, D., Cath, T.Y., Buisson, H., 2018. The role of nanotechnology in industrial water treatment. Nat. Nanotechnol. 13 (8), 670–672.
Jayakumar, A., Wurzer, C., Soldatou, S., Edwards, C., Lawton, L.A., Masek, O., 2021. New directions and challenges in engineering biologically-enhanced biochar for biological water treatment. Sci. Total. Environ. 796, 148977.
Ji, Y., Bai, J., Li, J., Luo, T., Qiao, L., Zeng, Q., Zhou, B., 2017. Highly selective transformation of ammonia nitrogen to $N_2$ based on a novel solar-driven photoelectrocatalytic-chlorine radical reactions system. Water Res 125, 512–519.
Ke, M.K., Huang, G.X., Mei, S.C., Wang, Z.H., Zhang, Y.J., Hua, T.W., Zheng, L.R., Yu, H. Q., 2021. Interface-promoted direct oxidation of p-arsanilic acid and removal of total arsenic by the coupling of peroxymonosulfate and Mn-Fe-mixed oxide. Environ. Sci. Technol. 55 (10), 7063–7071.
Kim, K.H., Choi, C.W., Choung, S., Cho, Y., Kim, S., Oh, C., Lee, K.S., Lee, C.L., Zhang, K., Han, J.W., Choi, S.Y., Park, J.H., 2022. Continuous oxygen vacancy gradient in $TiO_2$ photoelectrodes by a photoelectrochemical-driven “self-purification” process. Adv. Energy Mater. 12, 7.
Kim, S., Piao, G., Han, D.S., Shon, H.K., Park, H., 2018. Solar desalination coupled with water remediation and molecular hydrogen production: a novel solar water-energy nexus. Energy Environ. Sci. 11 (2), 344–353.
Koo, M.S., Cho, K., Yoon, J., Choi, W., 2017. Photoelectrochemical degradation of organic compounds coupled with molecular hydrogen generation using electrochromic $TiO_2$ nanotube arrays. Environ. Sci. Technol. 51 (11), 6590–6598.
Koo, M.S., Chen, X., Cho, K., An, T., Choi, W., 2019. In situ photoelectrochemical chloride activation using a $WO_3$ electrode for oxidative treatment with simultaneous $H_2$ evolution under visible light. Environ. Sci. Technol. 53 (16), 9926–9936.
Li, F., Sun, L., Liu, Y., Fang, X., Shen, C., Huang, M., Wang, Z., Dionysiou, D.D., 2020. A ClO• mediated photoelectrochemical filtration system for highly-efficient and complete ammonia conversion. J. Hazard. Mater. 400, 123246.
Li, H., Shang, J., Yang, Z., Shen, W., Ai, Z., Zhang, L., 2017. Oxygen vacancy associated surface fenton chemistry: surface structure dependent hydroxyl radicals generation and substrate dependent reactivity. Environ. Sci. Technol. 51 (10), 5685–5694.

Li, J., Pang, S.Y., Wang, Z., Guo, Q., Duan, J., Sun, S., Wang, L., Cao, Y., Jiang, J., 2021a. Oxidative transformation of emerging organic contaminants by aqueous permanganate: Kinetics, products, toxicity changes, and effects of manganese products. Water Res 203, 117513.
Li, X., Yu, J., Jaroniec, M., 2016. Hierarchical photocatalysts. Chem. Soc. Rev. 45 (9), 2603–2636.
Li, X., Kan, M., Wang, T., Qin, Z., Zhang, T., Qian, X., Kuwahara, Y., Mori, K., Yamashita, H., Zhao, Y., 2021b. The ClO• generation and chlorate suppression in photoelectrochemical reactive chlorine species systems on $BiVO_4$ photoanodes. Appl. Catal. B Environ. 296.
Li, X., Kan, M., Wang, T., Qin, Z., Zhang, T., Qian, X., Kuwahara, Y., Mori, K., Yamashita, H., Zhao, Y., 2021d. The ClO• generation and chlorate suppression in photoelectrochemical reactive chlorine species systems on $BiVO_4$ photoanodes. Appl. Catal. B Environ. 296, 120387.
Li, Z., Luo, L., Li, M., Chen, W., Liu, Y., Yang, J., Xu, S.M., Zhou, H., Ma, L., Xu, M., Kong, X., Duan, H., 2021c. Photoelectrocatalytic C-H halogenation over an oxygen vacancy-rich $TiO_2$ photoanode. Nat. Commun. 12 (1), 6698.
Lian, Z., Tao, Y., Liu, Y., Zhang, Y., Zhu, Q., Li, G., Li, H., 2020. Efficient self-driving photoelectrocatalytic reactor for synergistic water purification and $H_2$ evolution. ACS Appl. Mater. Interfaces 12 (40), 44731–44742.
Liao, W., Yang, J., Zhou, H., Murugananthan, M., Zhang, Y., 2014. Electrochemically self-doped $TiO_2$ nanotube arrays for efficient visible light photoelectrocatalytic degradation of contaminants. Electrochim. Acta 136, 310–317.
Lim, J., Yang, Y., Hoffmann, M.R., 2019. Activation of peroxymonosulfate by oxygen vacancies-enriched Cobalt-doped black $TiO_2$ nanotubes for the removal of organic pollutants. Environ. Sci. Technol. 53 (12), 6972–6980.
Lin, Y., Yang, C., Wu, S., Li, X., Chen, Y., Yang, W.L., 2020. Construction of built-in electric field within silver phosphate photocatalyst for enhanced removal of recalcitrant organic pollutants. Adv. Funct. Mater. 30 (38), 2002918.
Liu, Y., Pan, D., Xiong, M., Tao, Y., Chen, X., Zhang, D., Huang, Y., Li, G., 2020. In-situ fabrication $SnO_2/SnS_2$ heterostructure for boosting the photocatalytic degradation of pollutants. Chin. J. Cata. 41 (10), 1554–1563.
Liu, Y., Wang, Y., Wu, T., Xu, J., Lin, D., 2022. Synergistic effect of soil organic matter and nanoscale zero-valent iron on biodechlorination. Environ. Sci. Technol. 56 (8), 4915–4925.
Luo, T., Bai, J., Li, J., Zeng, Q., Ji, Y., Qiao, L., Li, X., Zhou, B., 2017. Self-driven photoelectrochemical splitting of $H_2S$ for S and $H_2$ recovery and simultaneous electricity generation. Environ. Sci. Technol. 51 (21), 12965–12971.
Ma, L., Gao, X., Liu, X., Gu, X., Li, B., Mao, B., Sun, Z., Gao, W., Jia, X., Chen, J., 2022. Recent advances in organic electrosynthesis using heterogeneous catalysts modified electrodes. Chin. Chem. Lett.
Mei, J., Tao, Y., Gao, C., Zhu, Q., Zhang, H., Yu, J., Fang, Z., Xu, H., Wang, Y., Li, G., 2021. Photo-induced dye-sensitized $BiPO_4$/BiOCl system for stably treating persistent organic pollutants. Appl. Cata. B Environ. 285, 119841.
Menzel, N., Ortel, E., Mette, K., Kraehnert, R., Strasser, P., 2013. Dimensionally stable Ru/Ir/$TiO_2$-Anodes with tailored mesoporosity for efficient electrochemical chlorine evolution. ACS Catal. 3 (6), 1324–1333.
Nosaka, Y., Nosaka, A.Y., 2017. Generation and detection of reactive oxygen species in photocatalysis. Chem. Rev. 117 (17), 11302–11336.
Pan, D., Xiao, S., Chen, X., Li, R., Cao, Y., Zhang, D., Pu, S., Li, Z., Li, G., Li, H., 2019. Efficient photocatalytic fuel cell via simultaneous visible-photoelectrocatalytic degradation and electricity generation on a porous coral-like $WO_3$/W photoelectrode. Environ. Sci. Technol. 53 (7), 3697–3706.
Pan, M., Tan, Y.Z., Chew, J.W., 2020. Superior membrane distillation by induction heating of 3D rGO/Nafion/Ni foam for water treatment. J. Membr. Sci. 616, 118609.
Park, J., Lee, T.H., Kim, C., Lee, S.A., Choi, M.-J., Kim, H., Yang, J.W., Lim, J., Jang, H. W., 2021. Hydrothermally obtained type-IIheterojunction nanostructures of $In_2S_3$/$TiO_2$ for remarkably enhanced photoelectrochemical water splitting. Appl. Cata. B Environ. 295, 120276.
Pu, S., Hou, Y., Yan, C., Ma, H., Huang, H., Shi, Q., Mandal, S., Diao, Z., Chu, W., 2018. In situ coprecipitation formed highly water-dispersible magnetic chitosan nanopowder for removal of heavy metals and its adsorption mechanism. ACS Sustain. Chem. Eng. 6 (12), 16754–16765.
Shao, D., Wu, Y., Hu, S., Gao, W., Du, Y., Jia, X., Liu, S., Zhou, M., Chen, J., 2022. Decoupled photoelectrochemical cerium-catalyzed oxydichlorination of alkynes: Slow releasing of chloride ions and chlorine radicals. ACS Sustain. Chem. Eng. 10 (31), 10294–10302.
Song, R., Chi, H., Ma, Q., Li, D., Wang, X., Gao, W., Wang, H., Wang, X., Li, Z., Li, C., 2021. Highly efficient degradation of persistent pollutants with 3D nanocone $TiO_2$-based photoelectrocatalysis. J. Am. Chem. Soc. 143 (34), 13664–13674.
Sözen, S., Olmez-Hanci, T., Hooshmand, M., Orhon, D., 2019. Fenton oxidation for effective removal of color and organic matter from denim cotton wastewater without biological treatment. Environ. Chem. Lett. 18 (1), 207–213.
Sun, J., Bi, H., Jia, H., Su, S., Dong, H., Xie, X., Sun, L., 2020. A low cost paper tissue-based PDMS/$SiO_2$ composite for both high efficient oil absorption and water-in-oil emulsion separation. J. Clean. Prod. 244, 118814.
Wang, G., Ling, Y., Wang, H., Yang, X., Wang, C., Zhang, J.Z., Li, Y., 2012. Hydrogen-treated $WO_3$ nanoflakes show enhanced photostability. Energy Environ. Sci. 5, 3.
Wang, S., Chen, P., Bai, Y., Yun, J.H., Liu, G., Wang, L., 2018a. New $BiVO_4$ Dual photoanodes with enriched oxygen vacancies for efficient solar-driven water splitting. Adv. Mater. 30 (20), e1800486.
Wang, S., Chen, P., Bai, Y., Yun, J.H., Liu, G., Wang, L., 2018b. New $BiVO_4$ Dual photoanodes with enriched oxygen vacancies for efficient solar-driven water splitting. Adv. Mater. 30 (20), 1800486.
Wang, W., Xu, M., Xu, X., Zhou, W., Shao, Z., 2020. Perovskite oxide based electrodes for high-performance photoelectrochemical water splitting. Angew. Chem. Int. Ed. 59 (1), 136–152.
Wang, Z., Mao, X., Chen, P., Xiao, M., Monny, S.A., Wang, S., Konarova, M., Du, A., Wang, L., 2019. Understanding the roles of oxygen vacancies in hematite-based photoelectrochemical processes. Angew. Chem. Int. Ed. 58 (4), 1030–1034.
Xiao, S., Wan, Z., Zhou, J., Li, H., Zhang, H., Su, C., Chen, W., Li, G., Zhang, D., Li, H., 2019. Gas-phase photoelectrocatalysis for breaking down nitric oxide. Environ. Sci. Technol. 53 (12), 7145–7154.
Xu, X., Cai, J., Zhou, M., Du, X., Zhang, Y., 2020. Photoelectrochemical degradation of 2,4-dichlorophenoxyacetic acid using electrochemically self-doped blue $TiO_2$ nanotube arrays with formic acid as electrolyte. J. Hazard. Mater. 382, 121096.
Zhang, X., Qin, J., Xue, Y., Yu, P., Zhang, B., Wang, L., Liu, R., 2014. Effect of aspect ratio and surface defects on the photocatalytic activity of ZnO nanorods. Sci. Rep. 4, 4596.
Zhang, Y., Li, J., Bai, J., Shen, Z., Li, L., Xia, L., Chen, S., Zhou, B., 2018. Exhaustive conversion of inorganic nitrogen to nitrogen gas based on a photoelectro-chlorine cycle reaction and a highly selective nitrogen gas generation cathode. Environ. Sci. Technol. 52 (3), 1413–1420.
Zhang, Y., Li, J., Bai, J., Li, L., Chen, S., Zhou, T., Wang, J., Xia, L., Xu, Q., Zhou, B., 2019. Extremely efficient decomposition of ammonia-N to $N_2$ Using ClO• from reactions of HO• and HOCl generated in situ on a novel bifacial photoelectroanode. Environ. Sci. Technol. 53 (12), 6945–6953.
Zhang, Y., Ji, Y., Li, J., Bai, J., Chen, S., Li, L., Wang, J., Zhou, T., Jiang, P., Guan, X., Zhou, B., 2021. Efficient ammonia removal and toxic chlorate control by using $BiVO_4/WO_3$ heterojunction photoanode in a self-driven PEC-chlorine system. J. Hazard. Mater. 402, 123725.
Zhao, X., Pan, D., Chen, X., Li, R., Jiang, T., Wang, W., Li, G., Leung, D.Y.C., 2019. g-$C_3N_4$ photoanode for photoelectrocatalytic synergistic pollutant degradation and hydrogen evolution. Appl. Surf. Sci. 467–468, 658–665.
Zheng, Z., Lo, I.M.C., 2021. Fabrication of $MoS_2$@BL-$BiVO_4$ photoanode with promoted charge separation for photoelectrochemical sewage treatment to simultaneously degrade PPCPs, disinfect E. coli, and produce $H_2$: performance, mechanisms, and influence factors. Appl. Cata. B Environ. 299, 120636.
Zheng, Z., He, J., Dong, C., Lo, I.M.C., 2021. Photoelectrochemical sewage treatment by sulfite activation over an optimized $BiVO_4$ photoanode to simultaneously promote PPCPs degradation, $H_2$ evolution and E. coli disinfection. Chem. Eng. J. 419, 129418.